Total and differential cross-section calculations for the double photoionization of the helium $1s2s\ ^{1,3}S$ states

J. Colgan and M. S. Pindzola
Department of Physics, Auburn University, Auburn, Alabama 36849
(Received 25 September 2002; published 30 January 2003)

We apply the time-dependent close-coupling method to the double photoionization of helium from its $1s2s\ ^{1,3}S$ metastable states. Total integral cross sections are in excellent agreement with other nonperturbative theories. Single and triple differential cross sections are also presented which show interesting differences with previous calculations from the $1s^2$ ground state of helium. This set of calculations provides a goal for experimentalists to measure absolute total and angular differential cross sections for double ionization processes from excited states of atoms.

DOI: 10.1103/PhysRevA.67.012711 PACS number(s): 32.80.Fb

I. INTRODUCTION

The double photoionization of helium has recently attracted intense interest from both theory and experiment. This is due to its fundamental importance since the final state of two electrons moving in the field of an atomic nucleus is the classic three-body problem. The recent development of pioneering new experimental techniques has also stimulated much work in this area.

The experimental measurements for the double photoionization of helium now encompass the full range of cross sections. Absolute total double photoionization cross sections have been measured [1] as well as single differential cross sections at 20 eV excess photon energy [2]. Recoil ion-momentum spectroscopy techniques [3,4] have been used to measure absolute triple differential cross sections for helium, also at 20 eV excess photon energy. Several other experimental groups have made detailed studies of the triple differential cross sections for helium, at various regimes of incident photon energy and energy sharing ratios of the two outgoing electrons [5–9].

Fortunately, in recent years, theory has managed to keep pace with these rapid experimental advances. Total and single energy differential cross sections for helium have been calculated using the double screened Coulomb method [10–12]. The convergent close-coupling method has successfully calculated total integral as well as single and triple differential cross sections for helium [16,17] and recently the hyperspherical *R*-matrix method has had great success in calculating single differential and triple differential cross sections for helium for a wide range of electron energy sharings [13–15]. The time-dependent close-coupling method [18–20] has also calculated total, single, and triple differential cross sections for helium. These three nonperturbative approaches have all demonstrated excellent agreement with each other and with experiment for all measurements made on helium to date, for a wide range of incident photon energies and energy sharings between the outgoing electrons. It seems that the double photoionization of the ground state of helium may be regarded as a well understood problem from both the theoretical and experimental viewpoint. In addition, the time-dependent and convergent close-coupling methods have calculated double photoionization cross sections for beryllium [21,22], although for this system no experimental measurements are available.

In this paper, we move on to examine double photoionization of helium from its excited $1s2s\ ^{1,3}S$ metastable states using the time-dependent close-coupling method. The first calculations of double photoioniation from a metastable state of helium were made by Teng and Shakeshaft [23], although they examined only very high photon energies. A study of the ratio of double to single photoionization for the helium isoelectronic sequence was made by Forrey *et al.* [24], where highly accurate Pekeris-type wave functions were used. Similarly, the ratio of double-to-single ionization from these states for helium has been calculated by van der Hart *et al.* [25,26] using a combined *R*-matrix *B*-spline approach. The calculations are in good agreement with convergent close-coupling calculations [27], which also calculated the absolute double ionization cross section. We find good agreement with these sets of calculations and also present angular differential cross sections for excited-state helium. Interesting differences are found in comparing these differential cross sections with those obtained from the ground state, as was also found in the high-energy calculations of [23]. It is hoped that this set of calculations can stimulate experimental activity in measuring cross sections for double ionization processes from excited states of atoms. Although this may be a major challenge to existing experimental setups, such measurements would be invaluable in exploring further the electron-electron correlations in such few-body systems.

In the following section, we present, briefly, the theory behind the time-dependent close-coupling method, and then we present a comprehensive selection of results for the double ionization of excited-state helium in Sec. III. We compare, where possible, with previous theoretical calculations. A summary and conclusions are given in Sec. IV.

II. TIME-DEPENDENT CLOSE-COUPLING THEORY

The time-dependent close-coupling theory describing double photoionization processes has been described in detail in previous work [18–20]. Here we give only a summary of the theory.

We begin with the time-dependent Schrödinger equation in real time:

$$i\frac{\partial \Psi^{1,3P}(\vec{r}_1,\vec{r}_2,t)}{\partial t} = H_{\rm atom}\Psi^{1,3P}(\vec{r}_1,\vec{r}_2,t) + H_{\rm rad}\Phi_0^{1,3S}(\vec{r}_1,\vec{r}_2)e^{-iE_0t}, \quad (1)$$

where we remember that the ^1S state is coupled to ^1P by the photon and that similarly the ^3S state is coupled to ^3P. The Hamiltonian for a linearly polarized radiation field in the length gauge is given by

$$H_{\rm rad} = E(t)(r_1\cos\theta_1 + r_2\cos\theta_2)\cos\omega t, \quad (2)$$

with electric-field amplitude $E(t)$ and radiation frequency ω. The electric field is ramped on smoothly over one-quarter of a field period so that $E(t)=t/T$ for $t<T/4$ and $E(t)=1$ for $t>T/4$. The velocity gauge was also used, and all the cross sections of helium presented here have been found to be gauge invariant.

The initial $\Phi_0^{1,3S}(\vec{r}_1,\vec{r}_2)$ state of helium is found by an expansion in coupled spherical harmonics and subsequent relaxation of the time-dependent Schrödinger equation (containing only the nonrelativistic Hamiltonian $H_{\rm atom}$) in imaginary time. This works well for the $1s2s\ ^3S$ state, which is the lowest possible state for this symmetry. However, in the ^1S case, the relaxation will result in the $1s^2\ ^1S$ state, since this has the same symmetry as the $1s2s\ ^1S$ state. Therefore, we must perform a Schmidt orthogonalization of the $1s2s\ ^1S$ state to the $1s^2\ ^1S$ state to arrive at the desired $1s2s\ ^1S$ state.

It was found that this relaxation of the time-dependent Schrödinger equation must be propagated for much longer than was necessary for the ground $1s^2$ state of helium. If not, the $1s2s$ state will still contain components of more highly excited states, so that one does not start from the pure $1s2s$ state. Relaxation for a longer period (up to 25 atomic units of time) ensures that a pure $1s2s$ state is calculated. We remark that this convergence can be tested by propagating this wave function in real time, with no field interaction, and periodically projecting it onto its $t=0$ value. A pure $1s2s$ state will give the same integral, whereas a $1s2s$ with some mixture of more highly excited states will give a value which oscillates about the true figure.

The time-dependent wave function $\Psi^{1,3P}(\vec{r}_1,\vec{r}_2,t)$ is also expanded in coupled spherical harmonics and the resulting set of coupled partial differential equations is solved on a numerical lattice with a mesh spacing of $\Delta r=0.1$ and time propagated for between 10 and 15 radiation field periods $(2\pi/\omega)$, depending on the excess photon energy. A lattice size of 600×600 points is employed. Increasing the lattice to 1000×1000 points made a difference of no more than 2% in any of the results presented here.

The total integral cross section for double photoionization is given by

$$\sigma_{\rm dion}^{1,3P} = \frac{\omega}{I}\frac{\partial \mathcal{P}^{1,3P}{}_{\rm dion}}{\partial t}, \quad (3)$$

where I is the radiation field intensity, and $P_{\rm dion}^{1,3P}$ is the probability for double ionization defined by

$$\mathcal{P}_{\rm dion}^{1,3P} = \sum_{l_1,l_2}\ \frac{2}{\pi}\int dk_1\ \frac{2}{\pi}\int dk_2\ |P_{l_1l_2}^{1,3P}(k_1,k_2,t)|^2, \quad (4)$$

where

$$P_{l_1l_2}^{1,3P}(k_1,k_2,t) = \int_0^\infty dr_1\int_0^\infty dr_2\ P_{k_1l_1}(r_1)P_{k_2l_2}(r_2) \times P_{l_1l_2}^{1,3P}(r_1,r_2,t), \quad (5)$$

and $P_{l_1l_2}^{1,3P}(r_1,r_2,t)$ are two-dimensional radial wave functions. The radial continuum states, $P_{kl}(r)$, are obtained on a fixed mesh in momentum space by integrating the radial Schrödinger equation for a Coulomb potential with $Z=2$ and normalizing to 1 times a sine function, for which $\Sigma_k \rightarrow (2/\pi)\int dk$. For most of the calculations presented here, 600 continuum state radial orbitals on a uniform momentum mesh were used, with a mesh spacing of typically 0.0025. A slightly larger mesh spacing was sometimes used in order to span a larger energy range for larger excess energy calculations.

We define the cross section for single photoionization with excitation to a bound state nl as

$$\sigma_{nl}^{1,3P} = \frac{\omega}{I}\frac{\partial \mathcal{P}_{nl}^{1,3P}}{\partial t}, \quad (6)$$

where we write

$$\mathcal{P}_{nl}^{1,3P} = \sum_{l_1,l_2}\left\{\frac{2}{\pi}\int_0^\infty dk_2\left|\int_0^\infty dr_1\int_0^\infty dr_2 \times P_{nl}(r_1)P_{k_2l_2}(r_2)P_{l_1l_2}^{1,3P}(r_1,r_2,t)\right|^2 + \frac{2}{\pi}\int_0^\infty dk_1\left|\int_0^\infty dr_1\int_0^\infty dr_2\ P_{k_1l_1}(r_1) \times P_{nl}(r_2)P_{l_1l_2}^{1,3P}(r_1,r_2,t)\right|^2\right\} \quad (7)$$

with $P_{nl}(r)$ a radial bound state. We can also calculate the double ionization probability by projecting the radial wave function onto suitable products of bound states and subtracting this from unity. The single photoionization with excitation cross section can also be calculated by this approach. We have checked our cross sections for double photoionization and for single photoionization with excitation using both methods and find excellent agreement between these two approaches.

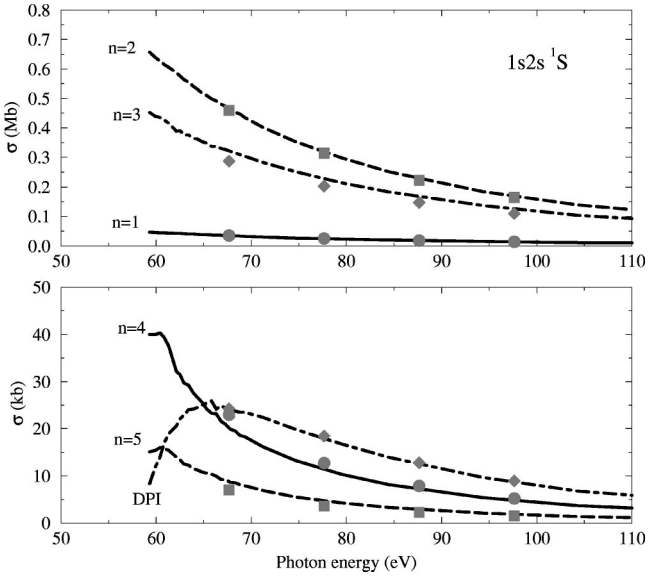

FIG. 1. Single photoionization with excitation cross sections for He $(1s2s)$ ^1S leaving the ion in the $n=1-5$ shells as indicated. The lines are the convergent close-coupling calculations [26] and the symbols are the present time-dependent close-coupling calculations. In the lower panel we also show the double photoionization cross section (indicated by DPI). Again we compare the convergent close-coupling (lines) and the time-dependent close-coupling (symbols) calculations. We note that the *y* axis for the lower panel is in kb. (1.0 Mb$=1.0\times10^{-18}$ cm^2, 1.0 kb$=1.0\times10^{-21}$ cm^2.)

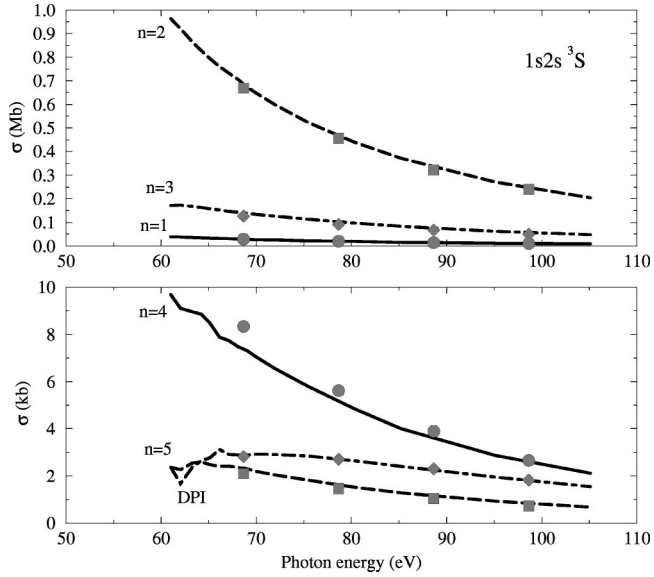

FIG. 2. Single photoionization with excitation cross sections for He $(1s2s)$ ^3S leaving the ion in the $n=1-5$ shells as indicated. The lines are the convergent close-coupling calculations [26] and the symbols are the present time-dependent close-coupling calculations. In the lower panel we also show the double photoionization cross section (indicated by DPI). Again we compare the convergent close-coupling (lines) and the time-dependent close-coupling (symbols) calculations. We note that the *y* axis for the lower panel is in kb. (1.0 Mb$=1.0\times10^{-18}$ cm^2, 1.0 kb$=1.0\times10^{-21}$ cm^2.)

The ejected-energy differential cross section may be defined as

$$\frac{d\sigma}{dE_1}=\frac{1}{k_1k_2}\frac{d\sigma}{d\alpha}, \tag{8}$$

where $d\sigma/d\alpha$ is the angle differential cross section in hyperspherical angle and integration of the differential cross section over all excess energy gives the total integral cross section. We remark here that this convention is different from the most commonly used convention where the ejected-energy differential cross section is defined from 0 to $E/2$.

The triple differential cross section for double photoionization is given by

$$\frac{d^3\sigma}{d\alpha d\Omega_1 d\Omega_2}=\frac{\omega}{I}\frac{\partial}{\partial t}\frac{2}{\pi}\int_0^\infty dk_1\,\frac{2}{\pi}\int_0^\infty dk_2 \times\delta\left(\alpha-\tan^{-1}\left(\frac{k_2}{k_1}\right)\right)\left|\sum_{l_1,l_2}(-i)^{l_1+l_2} \times e^{i(\sigma_{l_1}+\sigma_{l_2})}P^{1,3P}_{l_1l_2}(k_1,k_2,t)Y^{1,3P}_{l_1l_2}(\hat{k}_1,\hat{k}_2)\right|^2, \tag{9}$$

where σ_l is the Coulomb phase shift and $Y^{1,3P}_{l_1l_2}(\hat{k}_1,\hat{k}_2)$ are coupled spherical harmonics, and integration over all solid angles and ejected energy gives the total integral cross section.

III. RESULTS

A. Excitation-photoionization and double photoionization cross sections

We now compare the results of our calculations on He $(1s2s)$ with previous calculations. Time-dependent close-coupling calculations were carried out at 10, 20, 30, and 40 eV excess photon energies for both the ^1S and ^3S states, as described. The double photoionization cross sections and the single photoionization with excitation to a bound state were calculated for all energies. In Fig. 1, we show these calculations from the He $(1s2s)$ ^1S state along with the convergent close-coupling calculations of Kheifets *et al.* [27]. Cross sections for single photoionization with excitation to the $n=1-5$ states are shown, as well as double photoionization cross sections (labeled DPI). It is clear that the time-dependent calculations are in excellent agreement with the convergent close-coupling calculations for all the energies considered. The magnitude of the cross sections also clearly indicates that the ion is most likely to be left in the $n=2$ and $n=3$ states of He^+ after photoionization.

In Fig. 2, we show the corresponding calculations from the He $(1s2s)$ ^3S state, again comparing with the convergent close-coupling calculations of Kheifets *et al.* [27]. Again the agreement between the two sets of calculations is very good. We note that, for photoionization from this ^3S state, the ion is most likely to be left in the $n=2$ state. Ionization leaving the ion in the $n=4$ or $n=5$ state (or double photoionization) is much less probable (note that the scale on the *y* axis in the lower panel of both figures is in kb).

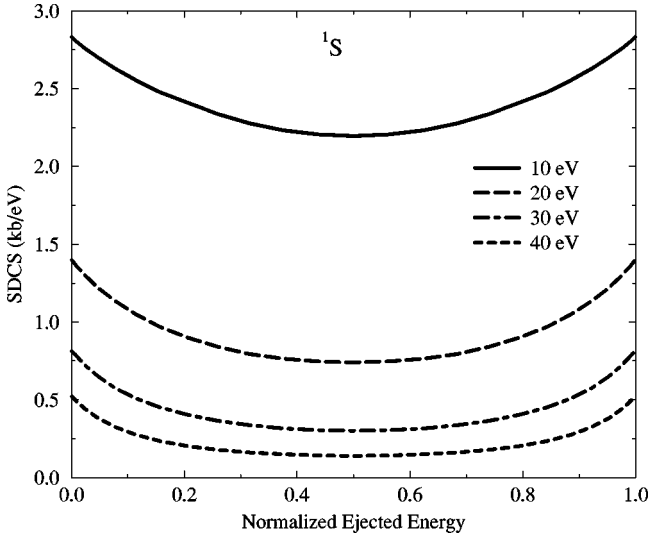

FIG. 3. Single differential cross sections in kb/eV for He ($1s2s$) ^1S at various excess photon energies as indicated. The cross section plots are such that the normalized ejected energy=ejected energy/excess energy. (1.0 kb=1.0×10^{-21} cm^2.)

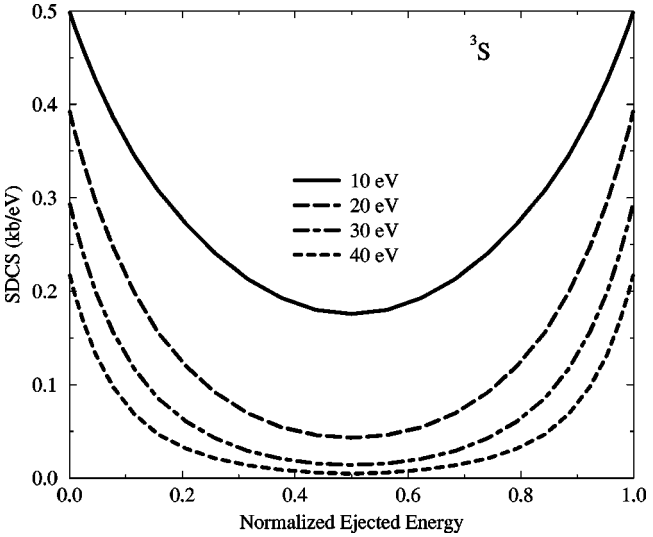

FIG. 4. Single differential cross sections in kb/eV for He ($1s2s$) ^3S at various excess photon energies as indicated. The cross section plots are such that the normalized ejected energy=ejected energy/excess energy. (1.0 kb=1.0×10^{-21} cm^2.)

For both these ^1S and ^3S cases, our calculations are also in good agreement with the calculations of van der Hart *et al.* [25], made using the combined *R*-matrix *B*-spline method.

It is also interesting to compare the magnitude of the double photoionization cross sections from the $1s2s$ ^1S and ^3S states with those from the ground $1s^2$ ^1S state (for example, Fig. 1 of [20]). The double ionization threshold for the $1s^2$ ^1S state is higher (around 79 eV) than from both $1s2s$ states (around 58 eV). Double photoionization from the $1s2s$ ^3S state has a peak cross section of around 3 kb at around an excess photon energy of 10 eV. For the double photoionization of $1s^2$ ^1S the cross section peaks at around 9 kb, at an excess photon energy of around 25 eV. The double photoionization of $1s2s$ ^1S has the largest cross section, with a peak of almost 25 kb, at around 10 eV excess photon energy. This reflects the fact that the $1s2s$ ^1S state is the most weakly bound of all three systems. We also note the large difference in the magnitude of the cross section between the $1s2s$ ^1S and ^3S states.

B. Single differential cross sections

In Figs. 3 and 4, we present single differential cross sections for double photoionization from the He $1s2s$ ^1S and ^3S states, respectively. We show cross sections at four different excess photon energies as before. For comparison we plot the single differential cross section against the normalized ejected energy (equal to ejected energy/excess energy). The magnitudes of the single differential cross sections reflect the total integral cross section at each excess photon energy (where in the convention used here, the area under the single differential cross-section curve from 0 to E equals the total integral cross section).

Again, it is interesting to compare these calculations with similar single differential cross-section calculations from He $1s^2$ ^1S (Fig. 2 of [20]). The most striking difference is that the single differential cross sections from the $1s2s$ ^1S and ^3S states are much more U-shaped than similar cross sections for the $1s^2$ ^1S state, which, by inspection of Fig. 2 of [20], are quite flat even at an excess photon energy of 60 eV. The more U-shaped nature may be understood since now the two ejected electrons are ionized from different shells and so they are less likely to be ejected with similar energies. Also, for the ^3S state, the cross sections are extremely U-shaped, even at the lowest photon energies considered. At the higher energies, the cross section at equal energy sharing between the electrons (where the normalized ejected energy=0.5) is almost zero. This is due to the large electron-electron repulsion present between two electrons in the same spin state, with equal outgoing energies. These results are also in agreement with the conclusions of the calculations of Teng and Shakeshaft [23], who considered much higher photon energies. It is clear that, for double photoionization from the ^3S state, the electrons are most likely to come out at very unequal energy sharings. Again we contrast this with the corresponding $1s^2$ case, where ejection at equal energies is almost as probable as at the unequal case, in the moderate photon energy range.

C. Triple differential cross sections

We now turn our attention to the triple differential cross sections which arise from our time-dependent close-coupling double photoionization calculations. In Figs. 5 and 6, we present the triple differential cross sections for helium $1s2s$ ^1S and ^3S, respectively, for an excess photon energy of 20 eV, for the case in which the excess energy is shared equally between the two ejected electrons. Cross sections are presented for various values of θ_1, the angle of the first ejected electron, as indicated, over a range of values of θ_2. As before, it is instructive to make comparisons with similar results for the ground $1s^2$ state of helium, for example Fig. 4

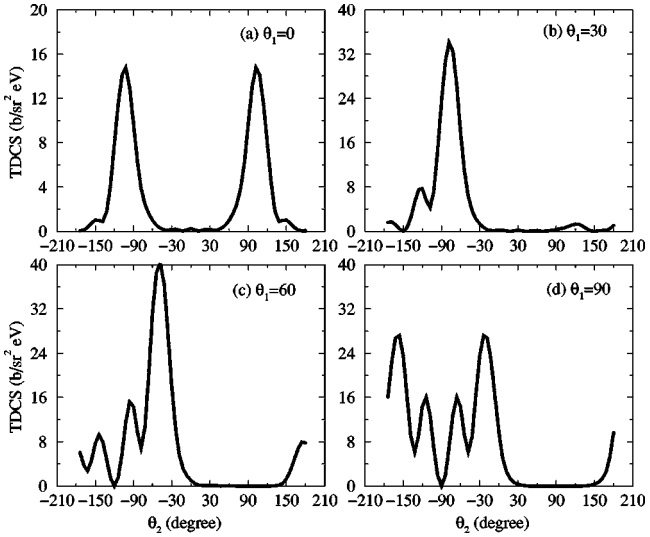

FIG. 5. Triple differential cross sections in b/sr^2 eV for helium $1s2s\ ^1S$ at 20 eV excess photon energy, for equal energy sharing ($E_1=E_2=10$ eV) between the two ejected electrons. We plot the cross section as a function of θ_2, the angle of the second ejected electron, for various values of θ_1 as indicated. (1.0 b $=1.0\times10^{-24}$ cm^2.)

of [19]. It is clear that the triple differential cross sections obtained for the $1s2s\ ^1S$ state are quite similar in shape to those obtained for the ground $1s^2$ state. The dominant peaks of the cross sections are in similar positions for both cases, as may be expected since we are ionizing from the same initial symmetry. However, we also see that the triple differential cross sections for the $1s2s\ ^1S$ state also show some further structure compared to the $1s^2$ state. For the three cases of $\theta_1=30°$, 60°, and 90°, extra peaks in the cross sections are seen, particularly in the backward scattering range. This extra structure is not an artifact of our calculations, since we have checked rigorously the convergence of our calculations, particularly with respect to the number of l_1l_2 channels included in our final state. In fact, it took 18 l_1l_2 pairs to fully converge these cross sections, compared to only eight pairs for the $1s^2$ ground state. This reflects the more diffuse nature of the $2s$ orbital. We also comment that calculations carried out in the velocity gauge give very similar results. It is difficult to determine the source of these extra structures in the $1s2s\ ^1S$ triple differential cross sections. They may be due to an added interference effect between the outgoing $1s$ and $2s$ electrons, which now arise from different shells, unlike the $1s2s$ case.

The corresponding case for the $1s2s\ ^3S$ case is shown in Fig. 6. Here the shape of the triple differential cross section is different from that of the two ^1S cases, which is to be expected since we start from an initial state of different symmetry. In fact, for the first three geometries only one large peak is present, at an angle of 180° from the first electron. It is clear that back-to-back ejection completely dominates the cross section for this case. The exception to this is the case in which $\theta_1=90°$, where we see that the cross section falls very sharply to zero at $\theta_2=-90°$, the back-to-back scattering angle. However, the large cross sections immediately before and after this angle show that back-to-back emission is still preferred, with the node at exactly $\theta_2=-90°$ arising purely from the zero in the coupled spherical harmonic at this angle. Thus the large peaks that characterize the triple differential cross sections for the $1s^2$ and $1s2s\ ^1S$ case are still present, although their position has been shifted more towards the backward scattering. This is a reflection of the extra repulsion present between the two electrons in the ^3S state. In this case, 14 l_1l_2 pairs were sufficient to con-

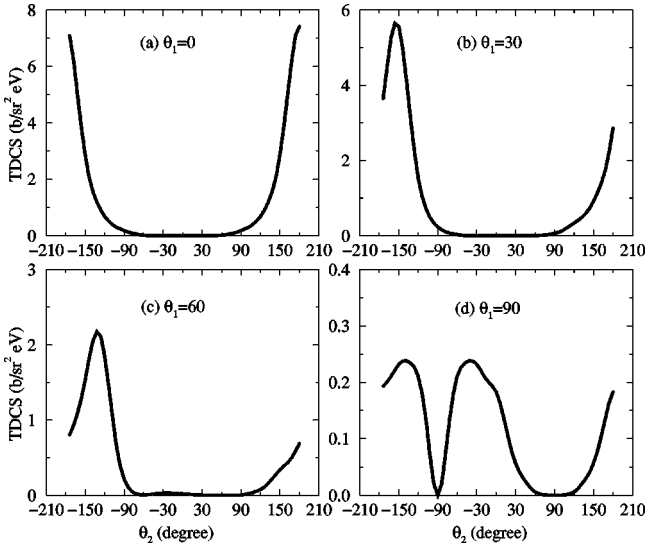

FIG. 6. Triple differential cross sections in b/sr^2 eV for helium $1s2s\ ^3S$ at 20 eV excess photon energy, for equal energy sharing ($E_1=E_2=10$ eV) between the two ejected electrons. We plot the cross section as a function of θ_2, the angle of the second ejected electron, for various values of θ_1 as indicated. (1.0 b $=1.0\times10^{-24}$ cm^2.)

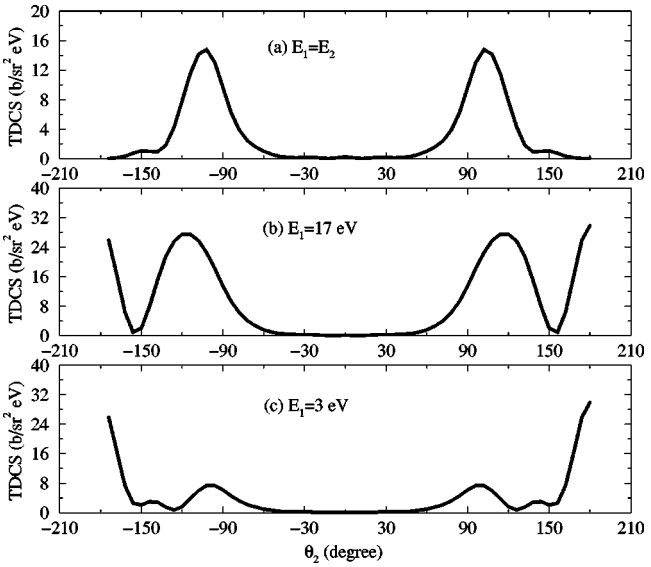

FIG. 7. Triple differential cross sections in b/sr^2 eV for helium $1s2s\ ^1S$ at 20 eV excess photon energy, for various energy sharings between the two ejected electrons as indicated, for $\theta_1=0°$, the angle of the first ejected electron. (1.0 b$=1.0\times10^{-24}$ cm^2.)

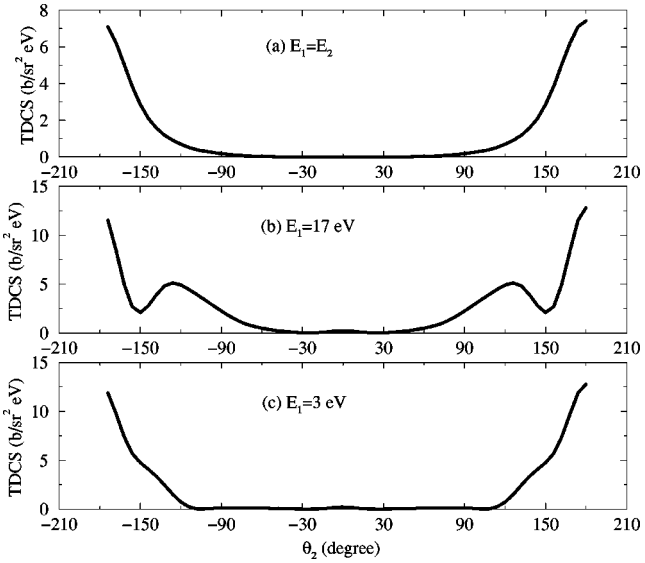

FIG. 8. Triple differential cross sections in b/sr^2 eV for helium $1s2s\ ^3S$ at 20 eV excess photon energy, for various energy sharings between the two ejected electrons as indicated, for $\theta_1=0°$, the angle of the first ejected electron. (1.0 b$=1.0\times10^{-24}$ cm^2.)

verge these cross sections, less than the $1s2s\ ^1S$ case, again because of the repulsion present because of the identical spin of the electrons.

In Figs. 7 and 8, we show triple differential cross sections from the helium $1s2s\ ^1S$ and ^3S states, for the case in which θ_1, the angle of the first ejected electron, is fixed at zero, for three different values of energy sharing between the ejected electrons, as shown. The top part of the figure is for equal energy sharing, the second is the case in which $E_1=17$ eV and $E_2=3$ eV, and the bottom shows the converse case in which $E_1=3$ eV and $E_2=17$ eV. Again we show these results to compare with previous calculations made from the helium ground $1s^2$ state [19], Fig. 5.

Again we see that the $1s^2\ ^1S$ and $1s2s\ ^1S$ cases are quite similar in the shape of the triple differential cross section. The peaks in the cross section for (b), $E_1=17$ eV and $E_2=3$ eV, are more pronounced for the $1s2s\ ^1S$ case. We also see an extra peak for this state in case (c), $E_1=3$ eV and $E_2=17$ eV, for $|\theta_2|=135°$. This is absent from the $1s^2\ ^1S$ case. For the triple differential cross section from the $1s2s\ ^3S$ state we again notice that the electron-electron repulsion of the outgoing electrons from a triplet state has pushed the dominant peak in the cross section to about 180°. The smaller peaks, which are evident in the cross sections from the $1s2s\ ^1S$ and $1s^2\ ^1S$ states, are also suppressed for this case.

IV. SUMMARY

In this paper, we have explored in detail the double photoionization of excited-state helium $1s2s\ ^{1,3}S$ using the time-dependent close-coupling method. This technique has previously been shown to give accurate results for all total and angular cross sections for the ground state of helium. Our calculations of the total double photoionization cross section and also single photoionization leaving the ion in an excited state have been shown to be in excellent agreement with other theoretical calculations made using the convergent close-coupling method and *R* matrix using *B*-spline technique.

We have also presented single energy differential cross sections for helium $1s2s$ from both metastable states and discussed the differences in these cross sections with those obtained from the ground state. Triple differential cross sections have also been calculated. Again, comparison is made with similar cross sections obtained from the helium ground state, and interesting differences are discussed. It is found that the more diffuse nature of the $2s$ orbital makes convergence of our calculations much more difficult. Also, possible interference effects between the $1s$ and $2s$ orbitals may give rise to added structure in the triple differential cross sections for helium $1s2s\ ^1S$.

Unfortunately there are no experimental measurements on helium from its excited state with which to compare these calculations. However, there have been some recent measurements of the double to single photoionization ratio for lithium [28,29], which have concentrated on the near-threshold region. We hope to make further calculations of the double photoionization of lithium in the near future in an effort to compare with these measurements. It is also hoped that this work will encourage experimental measurements of the angular differential cross sections discussed here to explore the interesting differences with such measurements made on ground-state helium.

ACKNOWLEDGMENTS

We would like to thank F. Robicheaux for valuable discussions and I. Bray for the communication of his results in numerical form. This work was supported in part by a grant from the Theoretical Division of the National Science Foundation, the Office of Fusion Energy Sciences of the U.S. Department of Energy, and the SciDAC program of the U.S. Department of Energy. Computational work was carried out at the Center for Computing Services, Oak Ridge National Laboratory, TN, and the National Energy Research Supercomputing Center, Oakland, CA.

[1] J.A.R. Samson, W.C. Stolte, Z.X. He, J.N. Cutler, Y. Lu, and R.J. Bartlett, Phys. Rev. A **57**, 1906 (1998).

[2] R. Wehlitz, F. Heiser, O. Hemmers, B. Langer, A. Menzel, and U. Becker, Phys. Rev. Lett. **67**, 3764 (1991).

[3] R. Dörner, T. Vogt, V. Mergel, H. Klemliche, S. Kravis, C.L. Cocke, J. Ullrich, M. Unverzagt, L. Spielberger, M. Damrau, O. Jagutski, I. Ali, B. Weaver, K. Ullmann, C.C. Hsu, M. Jung, E.P. Kanter, B. Sonntag, M.H. Prior, E. Rotenberg, J. Denlinger, T. Warwick, S.T. Manson, and H. Schmidt-Böcking, Phys. Rev. Lett. **76**, 2654 (1996).

[4] H. Bräuning, R. Dörner, C.L. Cocke, M.H. Prior, B. Krassig, A.S. Kheifets, I. Bray, A. Bräuning-Demian, K. Carnes, S. Dreuil, V. Mergel, P. Richard, J. Ullrich, and H. Schmidt-Böcking, J. Phys. B **31**, 5149 (1998).
[5] S. Cvejanović, J.P. Wightman, T.J. Reddish, F. Maulbetsch, M.A. MacDonald, A.S. Kheifets, and I. Bray, J. Phys. B **33**, 265 (2000).
[6] C. Dawson, S. Cvejanović, D. Seccombe, T.J. Reddish, F. Maulbetsch, A. Huetz, J. Mazeau, and A.S. Kheifets, J. Phys. B **34**, L525 (2001).
[7] J.P. Wightman, S. Cvejanović, and T.J. Reddish, J. Phys. B **31**, 1753 (1998).
[8] S.A. Collins, A. Huetz, T.J. Reddish, D.P. Seccombe, and K. Soejima, Phys. Rev. A **64**, 062706 (2001).
[9] P. Bolognesi, R. Camilloni, M. Coreno, G. Turri, J. Berakdar, A.S. Kheifets, and L. Avaldi, J. Phys. B **34**, 3193 (2001).
[10] D. Proulx and R. Shakeshaft, Phys. Rev. A **48**, R875 (1993).
[11] M. Pont, R. Shakeshaft, F. Maulbetsch, and J.S. Briggs, Phys. Rev. A **53**, 3671 (1996).
[12] M. Pont and R. Shakeshaft, J. Phys. B **28**, L571 (1995).
[13] L. Malegat, P. Selles, and A.K. Kazansky, Phys. Rev. A **60**, 3667 (1999).
[14] L. Malegat, P. Selles, and A.K. Kazansky, Phys. Rev. Lett. **85**, 4450 (2000).
[15] P. Selles, L. Malegat, and A.K. Kazansky, Phys. Rev. A **65**, 032711 (2002).
[16] A.S. Kheifets and I. Bray, J. Phys. B **31**, L447 (1998).
[17] A.S. Kheifets and I. Bray, Phys. Rev. A **62**, 065402 (2000).
[18] M.S. Pindzola and F. Robicheaux, Phys. Rev. A **57**, 318 (1998); **58**, 779 (1998).
[19] J. Colgan, M.S. Pindzola, and F. Robicheaux, J. Phys. B **34**, L457 (2001).
[20] J. Colgan and M.S. Pindzola, Phys. Rev. A **65**, 032729 (2002).
[21] J. Colgan and M.S. Pindzola, Phys. Rev. A **65**, 022709 (2002).
[22] A.S. Kheifets and I. Bray, Phys. Rev. A **65**, 012710 (2002).
[23] Z. Teng and R. Shakeshaft, Phys. Rev. A **49**, 3597 (1994).
[24] R.C. Forrey, H.R. Sadeghpour, J.D. Baker, J.D. Morgan III, and A. Dalgarno, Phys. Rev. A **51**, 2112 (1995).
[25] H.W. van der Hart, K.W. Meyer, and C.H. Greene, Phys. Rev. A **57**, 3641 (1998).
[26] H.W. van der Hart and L. Feng, J. Phys. B **34**, L601 (2001).
[27] A.S. Kheifets, A. Ipatov, M. Arifin, and I. Bray, Phys. Rev. A **62**, 052724 (2000).
[28] R. Wehlitz, J.B. Bluett, and S.B. Whitfield, Phys. Rev. A **66**, 012701 (2002).
[29] R. Wehlitz, J.B. Bluett, and S.B. Whitfield, Phys. Rev. Lett. **89**, 093002 (2002).